Robust storage qubits in ultracold polar molecules

Philip Gregory (✉ p.d.gregory@durham.ac.uk)
Durham University https://orcid.org/0000-0002-3628-8750
Jacob Blackmore
Durham University https://orcid.org/0000-0003-1145-4879
Sarah Bromley
NIST and University of Colorado https://orcid.org/0000-0002-8130-6276
Jeremy Hutson
University of Durham https://orcid.org/0000-0002-4344-6622
Simon Cornish
Durham University https://orcid.org/0000-0003-1407-4126

Article

Keywords: Long-lived Coherence, Singlet Rovibrational Ground State, Quantum Information, High-resolution Ramsey Spectrocospy, Hyperfine States, Differential Tensor Light Shift

Posted Date: March 17th, 2021

DOI: https://doi.org/10.21203/rs.3.rs-279402/v1

Version of Record: A version of this preprint was published at Nature Physics on September 9th, 2021.
See the published version at https://doi.org/10.1038/s41567-021-01328-7.

Robust storage qubits in ultracold polar molecules

Philip D. Gregory[1], Jacob A. Blackmore[1], Sarah L. Bromley[1], Jeremy M. Hutson[2], and Simon L. Cornish[1*]
[1] *Joint Quantum Centre (JQC) Durham-Newcastle, Department of Physics, Durham University, Durham, United Kingdom, DH1 3LE.*
[2] *Joint Quantum Centre (JQC) Durham-Newcastle, Department of Chemistry, Durham University, Durham, United Kingdom, DH1 3LE.*

Quantum states with long-lived coherence are essential for quantum computation, simulation and metrology. The nuclear spin states of ultracold molecules prepared in the singlet rovibrational ground state are an excellent candidate for encoding and storing quantum information. However, it is important to understand all sources of decoherence for these qubits, and then eliminate them, in order to reach the longest possible coherence times. Here, we fully characterise the dominant mechanisms for decoherence of a storage qubit in an optically trapped ultracold gas of RbCs molecules using high-resolution Ramsey spectroscopy. Guided by a detailed understanding of the hyperfine structure of the molecule, we tune the magnetic field to where a pair of hyperfine states have the same magnetic moment. These states form a qubit, which is insensitive to variations in magnetic field. Our experiments reveal an unexpected differential tensor light shift between the states, caused by weak mixing of rotational states. We demonstrate how this light shift can be eliminated by setting the angle between the linearly polarised trap light and the applied magnetic field to a magic angle of $\arccos(1/\sqrt{3}) \approx 55°$. This leads to a coherence time exceeding 6.9 s (90% confidence level). Our results unlock the potential of ultracold molecules as a platform for quantum computation.

Quantum coherence is a key resource [1], underpinning many prominent applications in quantum science and technology. These range from precision tests of fundamental physics [2], quantum metrology [3] and state-of-the-art atomic clocks [4] to quantum information processing [5], quantum simulation [6] and quantum thermodynamics [7]. Understanding the limits on quantum coherence is therefore of fundamental interest and technological importance. Cooling matter into the ultracold regime leads to long interrogation times coupled with exquisite experimental control, enabling quantum coherence to be investigated with incomparable precision.

Ultracold polar molecules [8, 9] combine the rich internal structure associated with molecular vibration and rotation with access to controllable long-range dipole-dipole interactions. These properties have stimulated a diverse range of proposed applications spanning the fields of quantum computation [10–14], quantum simulation [15–18], quantum-state controlled chemistry [19–21], and precision tests of fundamental physics [22–24]. To realise many of these applications, we need to understand how to engineer long-lived quantum coherence in ultracold polar molecules.

In this work, we use high-precision Ramsey spectroscopy to investigate the sources of decoherence in an optically trapped ultracold gas of ^{87}Rb^{133}Cs molecules (hereafter RbCs). We focus on superpositions of nuclear spin states of the singlet rovibrational ground state. Such superpositions are expected to be relatively insensitive to magnetic dephasing, as the magnetic moments of the nuclear spins are small in comparison to electronic magnetic moments. Furthermore, the nuclear spin states are expected to experience near-identical AC Stark shifts in an optical trap, so that dephasing associated with the nonuniform optical potential is also suppressed. These properties point to the possibility of long-lived coherence and make the nuclear spin states of ultracold polar molecules excellent candidates for robust storage qubits in quantum computing architectures [11, 12, 25]. In such proposals, gate operations may be performed using dipolar-exchange interactions [15, 17] following microwave excitation to an excited rotational state, while single-qubit rotations can be performed using two-photon microwave pulses [26–29]. Here, we demonstrate coherence times exceeding 6.9 s (90% confidence level) for the storage qubit, paving the way for the use of ultracold molecules as a platform for quantum computation.

To begin, we seek to identify pairs of nuclear spin states with identical magnetic moments that connect to a common excited rotational state, by calculating the rotational and hyperfine structure of the RbCs molecule in externally applied magnetic and optical fields [28–31]. We construct the Hamiltonian (see Methods) in a fully uncoupled basis set $|N, M_N\rangle\,|i_{\rm Rb}, m_{\rm Rb}\rangle\,|i_{\rm Cs}, m_{\rm Cs}\rangle$, where N represents the angular momentum of the molecule with its projection along the quantisation axis M_N, and $i_{\rm Rb} = 3/2, i_{\rm Cs} = 7/2$ denote the nuclear spins of Rb and Cs respectively, with their projections $m_{\rm Rb}, m_{\rm Cs}$. However, typical magnetic fields in our experiments are not high enough to decouple the rotational and nuclear angular momenta. Even when the laser is polarised along the magnetic field, the only good quantum number that can be used to describe a given hyperfine sublevel is $M_F = M_N + m_{\rm Rb} + m_{\rm Cs}$. As this is not sufficient to identify a given hyperfine state uniquely, we label the states by $(N, M_F)_k$ where k is an index counting up the states in order of increasing energy, such that $k = 0$ is the lowest-energy state for given values of N and M_F. There are 32

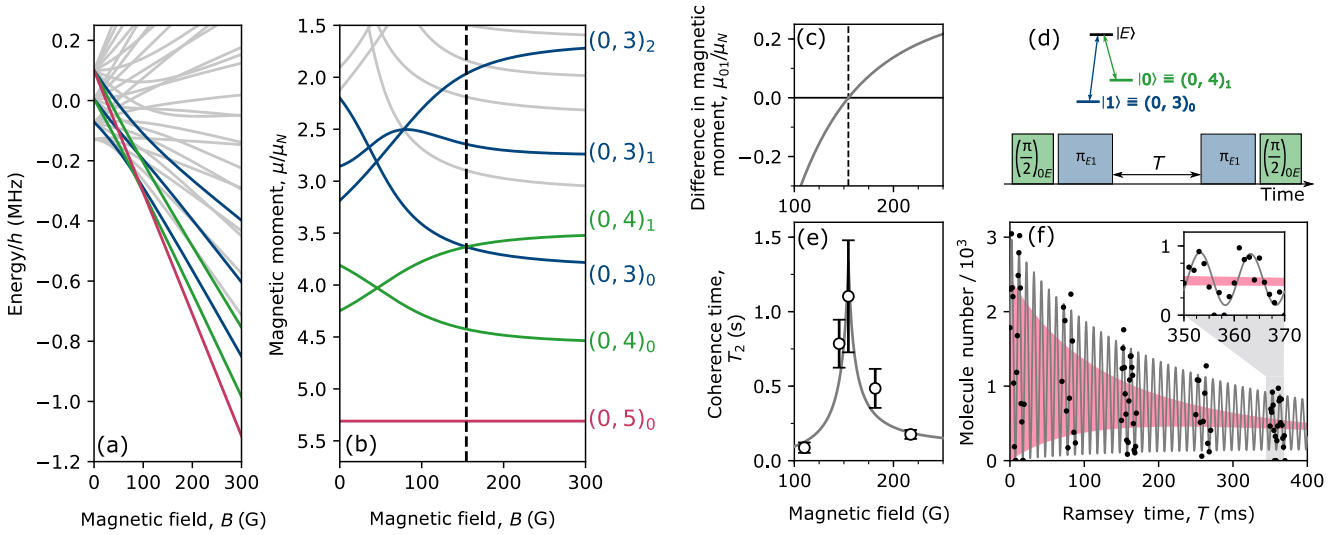

FIG. 1. **Effect of magnetic fields on the coherence of the storage qubit.** **(a)** Zeeman structure of the nuclear spin states in the rotational ground state of RbCs. **(b)** Magnetic moments μ/μ_N of the states as a function of magnetic field B. We construct the qubit from the states $|0\rangle \equiv (0,4)_1$ and $|1\rangle \equiv (0,3)_0$, which are chosen as they possess identical magnetic moments when $B = 154.524\,\mathrm{G}$ (indicated by the vertical dashed line). **(c)** The differential magnetic moment $\mu_{01} = \mu_{|1\rangle} - \mu_{|0\rangle}$ as a function of magnetic field. **(d)** Configuration of states and microwave pulse sequence used to perform Ramsey spectroscopy. The energy separation between the qubit states and the rotationally excited state $|E\rangle$ is $2B_v \approx 980\,\mathrm{MHz}$. **(e)** Measured coherence time T_2 as a function of magnetic field. The line shows a model for the decoherence as described in the text. Fitting to the results indicates a magnetic field variation of 34(5) mG over the course of the measurement contributes to the observed decoherence, and a peak coherence time $T_2^* = 1.3(4)\,\mathrm{s}$ when $\mu_{01} \approx 0$. **(f)** Example Ramsey measurement performed at $B = 154.50\,\mathrm{G}$, where $\mu_{01} \approx 0$. The y-axis indicates the number of molecules remaining in state $|0\rangle$ measured as a function of the Ramsey time T. The red shaded region indicates the maximum and minimum of the Ramsey fringes observed when $B = 217.39\,\mathrm{G}$, where $\mu_{01} \approx 0.17\,\mu_N$ and the coherence time is correspondingly much shorter. The trap light has polarisation $\beta = 0°$ and intensity $I = 15.8\,\mathrm{kW\,cm^{-2}}$ for all measurements shown.

nuclear spin states in the $N = 0$ rotational ground state of RbCs, with energies E shown in Fig. 1(a). The magnetic moments $\mu = dE/dB$ for a selection of the states are plotted as a function of magnetic field B in Fig. 1(b). There are a number of state combinations which display crossings where the difference in magnetic moments is zero. These crossings indicate turning points in the energy difference between states, where the energy difference becomes insensitive to magnetic field noise. Our experiment produces an optically trapped ultracold gas of RbCs molecules by association from a pre-cooled atomic mixture [32, 33], using a procedure (see Methods) that initialises the molecules in the state $(0,4)_1$; full state compositions are given in the Supplementary Information. For simplicity, we therefore select the qubit states to be $|0\rangle \equiv (0,4)_1$ and $|1\rangle \equiv (0,3)_0$ which are predicted to have the same magnetic moment when $B = 154.524\,\mathrm{G}$, as shown in Fig. 1(c), where we plot $\mu_{01} = \mu_{|1\rangle} - \mu_{|0\rangle}$.

We investigate the dependence of the coherence time T_2 on μ_{01} by performing a series of Ramsey measurements to measure T_2 as a function of B (see Fig. 1(d) and Methods). The results are shown in Fig. 1(e). We observe the longest coherence time when the difference in magnetic moments between the two states is zero, as expected. We fit the magnetic field variation of T_2 with

$$T_2 = \left(\frac{|\mu_{01}|\,\Delta B}{h} + \frac{1}{T_2^*} \right)^{-1}, \qquad (1)$$

where ΔB and T_2^* are fitting parameters (see the Supplementary Information for a derivation of Eq. 1). μ_{01} is calculated from the molecular Hamiltonian as shown in Fig. 1(c). ΔB describes the magnitude of variation in magnetic field over the duration of the measurement which contributes to the decoherence. We find $\Delta B = 34(5)\,\mathrm{mG}$, which is consistent with the expected stability of the magnetic fields in our experiments. The term T_2^* accounts for other sources of decoherence, which we show below to be dominated by differential tensor light shifts. For these measurements we find $T_2^* = 1.3(4)\,\mathrm{s}$, for trap light polarised with $\beta = 0°$ and intensity $I = 15.8\,\mathrm{kW\,cm^{-2}}$. Fig. 1(f) shows Ramsey fringes recorded close to the $\mu_{01} = 0$ condition and contrasts the behaviour with that seen at $B = 217.39\,\mathrm{G}$ where, although the difference in magnetic moments is still small, magnetic dephasing limits the coherence time. We estimate that the limit on the coherence time at $B = 154.52\,\mathrm{G}$ due to magnetic field noise of $\Delta B = 35\,\mathrm{mG}$ is $\sim 2.0 \times 10^3\,\mathrm{s}$ (see Supplementary Information).

To show that the remaining decoherence T_2^* is dom-

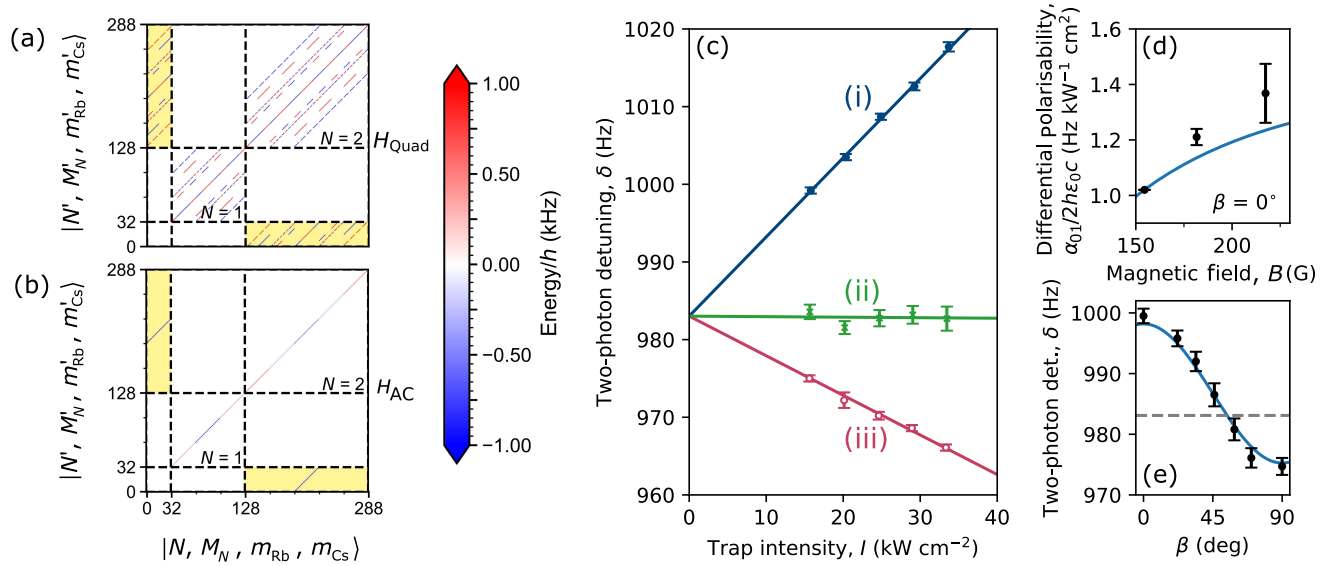

FIG. 2. **Differential tensor light shifts between nuclear spin states in the rotational ground state.** We measure the differential light shifts between $|0\rangle \equiv (0,4)_1$ and $|1\rangle \equiv (0,3)_0$ by Ramsey spectroscopy. We show the Hamiltonian matrix elements for **(a)** the nuclear electric quadrupole interaction $H_{\rm quad}$ and (b) the AC Stark effect $H_{\rm AC}$ graphically for the uncoupled $|N, M_N, m_{\rm Rb}, m_{\rm Cs}\rangle$ basis. The states are split by dashed lines into groups according to N and by minor ticks into multiples of 32 basis states with the same M_N. The block diagonal elements in N are labelled for $N > 0$. The color coding indicates the value of the matrix element in units of frequency. Note the off-diagonal elements connecting states with $\Delta N = 2$ shaded in yellow, which lead to tensor light shifts proportional to the anisotropic polarisability. The mathematical expressions describing the matrix elements are given in the Supplementary Information. $H^{(2)}_{\rm AC}$ is calculated for an intensity of 16 kW cm^{-2} and a polarisation angle of $\beta = 0°$. **(c)** Two-photon detuning δ as a function of the trap intensity I. The linear polarisation of each beam is set to an angle β of (i) 0° (ii) 55° (iii) 90° with respect to a 154.50 G magnetic field. The coloured lines indicate a fit to the results, following the model given in Eq. 3. We find $\alpha^{(2)}/(4\pi\epsilon_0) = 545(4)\, a_0^3$, and $\delta_0 = 983.0(2)$ Hz. **(d)** Differential polarisability between the states as a function of magnetic field, measured for $\beta = 0°$. The line is the expectation from the molecular Hamiltonian (see Methods). **(e)** δ measured in a single beam of the dipole trap with fixed intensity $I = 15.3$ kW cm^{-2}, as a function of β. The dashed horizontal line indicates δ_0. The solid line is calculated using Eq.3 with the parameters found in (c).

inated by differential tensor light shifts, we perform a series of Ramsey measurements using different optical trap intensities. Each Ramsey measurement allows us to precisely determine the difference in energy between $|0\rangle$ and $|1\rangle$. For these experiments the two microwaves fields differ in frequency by 76 kHz, and so by measuring the frequency of the Ramsey fringes δ, we determine the difference in energy between the states equal to $h \times (76\,\text{kHz} + \delta)$. The sign of δ is found by comparison with additional Ramsey measurements with intentionally different two-photon detunings. We measure δ for a range of trap laser intensities, and find an intensity-dependent energy shift between the two states as shown in Fig. 2.

The differential light shift arises from terms off-diagonal in N which cause mixing between states with the same parity. The largest contributions to the light shift are second-order terms

$$\langle N = 0, M_N = 0 |\, H_{\rm AC}\, | 2, 0\rangle \langle 2, 0 |\, H_{\rm quad}\, | 0, 0\rangle\,, \qquad (2)$$

where $H_{\rm AC}$ and $H_{\rm quad}$ represent the the AC Stark and nuclear electric quadrupole interactions, respectively (see Methods). The matrix elements of $H_{\rm AC}$ and $H_{\rm quad}$ are shown graphically in Figs. 2(a) and (b). These second-order terms lead to components with $N > 0$ in the state composition of $|0\rangle$ and $|1\rangle$ with coefficients $< 10^{-5}$. This results in tensor light shifts in the rotational ground state which scale with the anisotropic polarisability $\alpha^{(2)}$ [30] and depend on M_F and the laser polarisation. This is analogous to the tensor light shifts that arise in ground-state alkali atoms due to hyperfine structure [34]. The terms in Eq. 2 are all diagonal in M_N and are proportional to $P_2(\cos\beta) = \frac{1}{2}(3\cos^2\beta - 1)$, where β is the angle between the linearly polarised electric field of the trap light and the applied magnetic field which forms the quantisation axis. As a result, the light shift changes the observed two-photon detuning according to

$$\delta = (\alpha_{01} I)/2h\epsilon_0 c + \delta_0, \qquad (3)$$

where

$$\alpha_{01} = X(B)\alpha^{(2)} P_2(\cos\beta), \qquad (4)$$

is the difference in the effective differential polarisability

between the states. Here, I is the average intensity experienced by the molecules, δ_0 is the two-photon detuning in free space, and $X(B)$ is a numerical factor which is determined from the molecular Hamiltonian and depends upon the magnetic field.

In addition to the tensor light shift, each state also experiences a much larger scalar light shift. However, as the scalar shift is identical for all states, this does not contribute to decoherence. The largest differential tensor light shift we measure is $1.01995(6)\,\mathrm{Hz\,kW^{-1}\,cm^2}$, for $\beta = 0°$. This is caused by individual tensor lights shifts for each of the states which we calculate to be $-1.45\,\mathrm{Hz\,kW^{-1}\,cm^2}$ for $|0\rangle$, and $-2.47\,\mathrm{Hz\,kW^{-1}\,cm^2}$ for $|1\rangle$. In contrast the scalar light shift for both states is $-41.2\,\mathrm{kHz\,kW^{-1}\,cm^2}$; this is 4 orders of magnitude larger than the tensor light shifts.

We compare our calculations with the behaviour observed in experiments. For a magnetic field of $B \approx 154.50\,\mathrm{G}$ where magnetic decoherence is minimised, we calculate the prefactor $X(B) = 4.00(4) \times 10^{-5}$. We plot the differential light shift measured at this magnetic field in the optical trap for fixed laser polarisations $\beta = 0°, 54°, 90°$ in Fig. 2(c). The solid lines indicate a fit to the results using Eq. 3, with $\alpha^{(2)}$ and δ_0 as free parameters. We find excellent agreement between our model and the experiment, with $\alpha^{(2)}/4\pi\epsilon_0 = 545(4)\,a_0^3$ and $\delta_0 = 983.0(2)\,\mathrm{Hz}$. The uncertainties shown are the statistical uncertainties found in the fitting. Additional systematic uncertainties in $\alpha^{(2)}$ are given in the Supplementary Information. The value of δ_0 indicates the two-photon detuning in free space, and so we determine the free-space energy difference between the states of $h \times (76\,\mathrm{kHz} + \delta_0) = h \times 76.983\,0(2)\,\mathrm{kHz}$. This is in excellent agreement with a calculation from the molecular Hamiltonian which predicts an energy difference between the states of $h \times 77.0(7)\,\mathrm{kHz}$, where the uncertainty results from the current precision with which the strength of the scalar nuclear spin-spin interaction (c_4) and the magnitude of the nuclear magnetic moments are known for RbCs [28, 29].

To test our understanding of the origin of the differential light shift further, we explore different magnetic fields as shown in Fig. 2(d). For higher magnetic fields, the measurements are performed for $\beta = 0°$ only. The increased uncertainties arise from the magnetic dephasing restricting the measurement time. The variation with magnetic field arises from the numerical prefactor $X(B)$ in Eq. 4. We find good qualitative agreement between theory and experiment, with α_{01} rising with magnetic field. For calculations over a broader range of magnetic fields see the Supplementary Information. Our theory appears to underestimate the increase in α_{01} slightly. We attribute the discrepancy to uncertainties in the parameters of the molecular Hamiltonian which combine in a non-trivial way in the calculation of $X(B)$. Ramsey measurements of the type presented here should permit further refinement of these parameters. This will be the focus of future work.

The tensor light shifts we observe are proportional to $P_2(\cos\beta)$. This allows us to engineer a magic polarisation trap, as $P_2(\cos\beta) = 0$ for the magic angle $\beta_{\mathrm{magic}} = \arccos\sqrt{1/3} \approx 55°$. We experimentally verify this angle dependence in Fig. 2(e) using a single beam of the dipole trap. We see that the polarisation dependence of the experimentally measured δ is well described by our model and that $\delta \approx \delta_0$ when $\beta \approx 55°$, indicating that the tensor light shift is zero. This is further confirmed using the measurements in Fig. 2(c), where all δ measured in the trap for $\beta = 55°$ are consistent with the free-space value, and the gradient of δ as a function of I is zero.

The optimal configuration to maximise coherence time is where $\mu_{01} = 0$ and $\alpha_{01} = 0$, which is realised in our experiments for $B \approx 154.5\,\mathrm{G}$ and $\beta \approx 55°$. We perform a Ramsey experiment using these optimal parameters as shown in Fig. 3. The maximum Ramsey time available is limited by collisional loss of the molecules [35, 36] with $T_1 = 0.61(4)$ seconds, which reduces our signal at long times. We measure Ramsey fringes out to $T = 1.2\,\mathrm{s}$ with no evidence of decoherence. These results are consistent with $T_2^* > 6.9\,\mathrm{s}$ (90 % confidence level, see Supplementary Information), an order of magnitude longer than any previous work [25]. Using this measurement we find the energy difference between the states in the trap to be $h \times 76,982.733(16)\,\mathrm{Hz}$; this is a precision of 1 part in 10^7.

Our measurements do not indicate any other detectable mechanisms for decoherence. We see no evidence for collisional energy shifts, which would be observed by a change in the energies of the states when the density reduces over the course of each Ramsey measurement (see Supplementary Information). This is consistent with previous observations [25], and the absence of collisional energy shifts or decoherence may be expected as short-range collisions in the gas lead to loss of molecules with high probability [35–38]. Measurements of the coherence out to longer times will require confinement of the molecules to a 3D optical lattice [39] , optical tweezers [40–42], or the use of alternative trapping techniques such as a blue-detuned optical trap [43] to avoid losses from the optical excitation of two-molecule collision complexes [36, 44]. The creation of controlled arrays of molecules is also a key component of the proposed quantum computing protocols where storage qubits have applications; our method of using a magic-polarisation trap is compatible with the confinement of molecules to arrays of optical tweezers or a 3D optical lattice [45].

In conclusion, we have demonstrated a robust storage qubit constructed from the nuclear spin states of ultracold RbCs molecules. We have shown how magnetic dephasing can be eliminated by tuning the magnetic field to where the states have identical magnetic moments. This revealed an unexpected differential tensor light shift due to weak mixing of rotational states of the same parity,

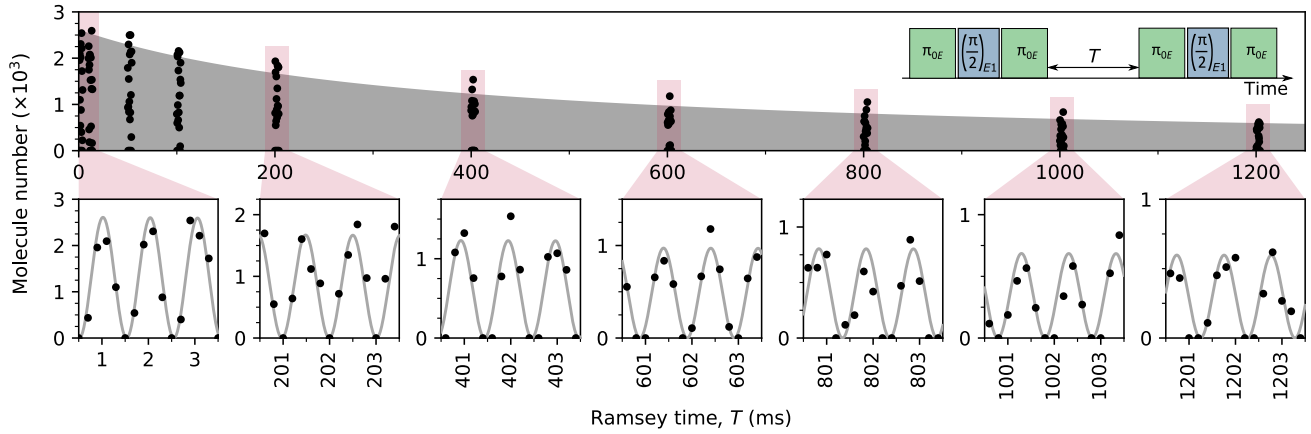

FIG. 3. **Robust coherence of the storage qubit.** Ramsey experiment with the qubit states $|0\rangle \equiv (0,4)_1$ and $|1\rangle \equiv (0,3)_0$, using the optimal configuration $B \approx 154.50\,\mathrm{G}$, $\beta \approx 55°$. The y-axis indicates the number of molecules remaining in $|0\rangle$, following the Ramsey sequence shown inset, as a function of the hold time T. The shaded region in the upper plot indicates the maximum and minimum of the Ramsey fringes as a function of time; the spacing of the fringes is too small to plot at this scale. The lower plots show the Ramsey fringes observed at 400 ms intervals.

which caused decoherence due to the nonuniform optical potential. We have shown how to eliminate these light shifts by setting the linear polarisation of the trap light to a magic angle $\beta_{\mathrm{magic}} = \arccos\sqrt{1/3} \approx 55°$ with respect to the magnetic field. Our optimal configuration leads to Ramsey fringes which persist for $T_2^* > 6.9\,\mathrm{s}$ (90 % confidence level), at least an order of magnitude improvement over the previous state of the art. Our findings are broadly applicable to all $^1\Sigma$ molecules in their rovibrational ground state, including the range of bialkali molecules currently under investigation. Our work demonstrates the implementation of robust storage qubits, which will be essential in future high-fidelity quantum computing architectures using controllable arrays of ultracold polar molecules.

METHODS

Hamiltonian used to calculate the rotational and hyperfine structure

We calculate the energy level structure of RbCs in the electronic and vibrational ground state by diagonalising the relevant Hamiltonian. We extract the energy levels and eigenstates of the Hamiltonian by numerical diagonalisation. The hyperfine constants for all of our calculations are given in the Supplementary Information. In the presence of externally applied magnetic and off-resonant optical fields, the Hamiltonian (H_{RbCs}) can be decomposed into rotational (H_{rot}), hyperfine (H_{hf}), Zeeman (H_{Zeeman}), and AC Stark (H_{AC}) components [46, 47]:

$$H_{\mathrm{RbCs}} = H_{\mathrm{rot}} + H_{\mathrm{hf}} + H_{\mathrm{Zeeman}} + H_{\mathrm{AC}}. \tag{5}$$

The rotational contribution

$$H_{\mathrm{rot}} = B_v \boldsymbol{N}^2 - D_v \boldsymbol{N}^2 \cdot \boldsymbol{N}^2, \tag{6}$$

is defined by the rotational angular momentum operator $\boldsymbol{N}$, and the rotational and centrifugal distortion constants, B_v and D_v. The hyperfine contribution consists of four terms

$$H_{\mathrm{hf}} = H_{\mathrm{quad}} + H_{II}^{(0)} + H_{II}^{(2)} + H_{NI}, \tag{7}$$

where

$$H_{\mathrm{quad}} = \sum_{j=\mathrm{Rb,Cs}} e\boldsymbol{Q}_j \cdot \boldsymbol{q}_j, \tag{8a}$$

$$H_{II}^{(0)} = c_4 \boldsymbol{I}_{\mathrm{Rb}} \cdot \boldsymbol{I}_{\mathrm{Cs}}, \tag{8b}$$

$$H_{II}^{(2)} = -c_3\sqrt{6}\boldsymbol{T}^2(C) \cdot \boldsymbol{T}^2(\boldsymbol{I}_{\mathrm{Cs}}, \boldsymbol{I}_{\mathrm{Rb}}) \tag{8c}$$

$$H_{NI} = \sum_{j=\mathrm{Rb,Cs}} c_j \boldsymbol{N} \cdot \boldsymbol{I}_j. \tag{8d}$$

H_{quad} represents the interaction between the nuclear electric quadrupole of nucleus j ($e\boldsymbol{Q}_j$) with the electric field gradient at the nucleus ($\boldsymbol{q}_j$). $H_{II}^{(0)}$ and $H_{II}^{(2)}$ are the scalar and tensor nuclear spin-spin interactions, with strengths governed by the coefficients c_4 and c_3. The second-rank tensors $\boldsymbol{T}^2$ describe the angular dependence and anisotropy of the interactions [48]. H_{NI} is the interaction between the nuclear magnetic moments and the magnetic field generated by the rotating molecule and has a coupling constant c_j for each of the two nuclei.

The Zeeman contribution to the Hamiltonian describes interaction of the rotational and nuclear magnetic moments with the external magnetic field ($\boldsymbol{B}$) and is

$$H_{\mathrm{Zeeman}} = -g_{\mathrm{r}}\mu_{\mathrm{N}}\boldsymbol{N} \cdot \boldsymbol{B} - \sum_{j=\mathrm{Rb,Cs}} g_j\,(1-\sigma_j)\,\mu_{\mathrm{N}}\boldsymbol{I}_j \cdot \boldsymbol{B}. \tag{9}$$

The first term accounts for the magnetic moment generated by the rotation of the molecule, characterised by the rotational g-factor g_r. The second term accounts for the nuclear spin contributions, characterised by the nuclear g-factors g_j shielded isotropically by the factor σ_j [47]. In both terms μ_N is the nuclear magneton. For our analysis we designate the axis of the magnetic field $\boldsymbol{B}$ as the space-fixed z axis and its magnitude as B.

The AC Stark effect arises from the interaction of an off-resonant oscillating electric field $\boldsymbol{E}_\mathrm{AC}$ with the frequency-dependent molecular polarisability tensor $\boldsymbol{\alpha}$ [30], and has a contribution to the Hamiltonian

$$H_\mathrm{AC} = -\frac{1}{2}\boldsymbol{E}_\mathrm{AC}\cdot\boldsymbol{\alpha}\cdot\boldsymbol{E}_\mathrm{AC}. \tag{10}$$

The terms H_quad, $H_{II}^{(2)}$, and H_AC all have components which are off-diagonal in N, and therefore contribute to the tensor light shifts which we observe. To be explicit, the matrix elements for these terms are included in Supplementary Information.

Production of ultracold RbCs molecules

We produce ground-state RbCs molecules from an optically trapped ultracold mixture of ^{87}Rb and ^{133}Cs atoms using a two-step process. First, we use magnetoassociation on an interspecies Feshbach resonance at 197 G [49]. Following this, the remaining atoms are removed from the trap using the Stern-Gerlach effect. Second, the magnetic field is set to 181.6 G, where the molecules are transferred to a single hyperfine sublevel of the $X^1\Sigma\,(v=0, N=0)$ rovibrational ground state using stimulated Raman adiabatic passage (STIRAP) [32, 33, 50]. We set the STIRAP to initialise the molecules in $|0\rangle \equiv (0,4)_1$, and the transfer is performed in free space to avoid spatially varying AC Stark shifts which otherwise limit the efficiency [33]. Following STIRAP, the molecules are recaptured in a crossed optical dipole trap at $\lambda = 1550$ nm; see the Supplementary Information for details. Both beams are linearly polarised at an angle β with respect to the applied magnetic field. The molecules have a typical temperature of 0.7 μK, and a peak density of $\sim 1\times10^{11}\,\mathrm{cm}^{-3}$. We detect molecules by reversing the creation process and imaging the resulting atomic clouds. As such, we only image molecules which occupy $|0\rangle$.

Ramsey measurement protocol

To measure the coherence time of the qubit, we perform Ramsey spectroscopy. To couple the qubit states, we use two microwave fields to form a 3-level lambda system, where both qubit states are coupled to a common rotationally excited state $|E\rangle$, which is chosen to have significant transition dipole moment to both $|0\rangle$ and $|1\rangle$. The excited states used throughout this work are tabulated in the Supplementary Information, along with technical details of the microwave apparatus we use.

For the measurements presented in Fig. 1, we prepare an equal superposition of $|0\rangle$ and $|1\rangle$ by applying a $\pi/2$ pulse on the $|0\rangle \leftrightarrow |E\rangle$ transition followed by a π pulse on the $|E\rangle \leftrightarrow |1\rangle$ transition. The optical trap is briefly switched off during any microwave pulses in order to avoid varying AC Stark shifts of the transitions across the thermal spatial distribution of molecules. The typical duration for each pulse is $\sim 100\,\mu$s. We project the phase of the superposition onto the population of the states by reversing this pulse sequence after a hold time T as shown in Fig.1(d). During T the molecules are confined to the crossed optical dipole trap, and a DC magnetic field is applied in the vertical z direction. With the two microwave frequencies fixed, we observe Ramsey fringes in the form of an oscillating number of molecules in the initial state $|0\rangle$ as a function of T.

For the measurements presented in Fig. 2 and Fig. 3, we find that there is a strong transition from $|0\rangle$ to $(1,4)_4$ just 20 kHz detuned from the $|E\rangle \leftrightarrow |1\rangle$ transition frequency. We therefore use a modified Ramsey sequence as shown in the inset to Fig. 3 to avoid off-resonantly driving the population out of $|0\rangle$ during the Ramsey pulses.

The frequency of the Ramsey fringes is equal to the two-photon detuning of the microwaves. We fit a model to the fringes (derived in Suppplementary Information) which accounts for both two-body collisional loss of molecules and decoherence of the superposition,

$$N(T) = \frac{N_i}{2}\left(\frac{1}{1+\frac{T}{T_1}[e-1]}\right)\times\left[e^{-T/T_2}\cos(2\pi(\delta T+\phi))+1\right]. \tag{11}$$

Here, N_i is the initial total number of molecules, T_1 is the $1/e$ lifetime for molecules in the trap, T_2 is the $1/e$ coherence time, and δ and ϕ are the frequency and phase of the Ramsey fringes.

To set the magnetic field for a given measurement, we jump the magnetic field to its target value immediately after the STIRAP and then hold 5 ms before the start of the Ramsey sequence. After the Ramsey sequence is completed, the magnetic field is jumped back to 181.6 G and held for 5 ms before the return STIRAP and imaging.

ACKNOWLEDGEMENTS

The authors thank M. R. Tarbutt for useful discussions and helpful comments on the early stages of the manuscript. We also thank I. G. Hughes for discussions with regard to the analysis of uncertainties and suggesting the use of the Feldman-Cousins approach. This work

was supported by U.K. Engineering and Physical Sciences Research Council (EPSRC) Grants EP/P01058X/1 and EP/P008275/1.

DATA AVAILABILITY

The data associated with this work are available at: **DOI to be added**.

CODE AVAILABILITY

The python code for hyperfine structure calculations can be found at **DOI:10.5281/ZENODO.3755881**.

AUTHOR CONTRIBUTIONS

P.D.G., J.A.B., S.L.B., and S.L.C. conceived the idea and planned the experiments. P.D.G. and J.A.B. performed the experiments and carried out the data analysis. J.A.B. wrote the code for calculating the rotational and hyperfine structure of the molecules with guidance from J.M.H.. All authors contributed to interpreting the results and the writing of the manuscript.

* s.l.cornish@durham.ac.uk

[1] A. Streltsov, G. Adesso, and M. B. Plenio, Colloquium: Quantum coherence as a resource, Rev. Mod. Phys. **89**, 041003 (2017).

[2] M. S. Safronova, D. Budker, D. DeMille, D. F. J. Kimball, A. Derevianko, and C. W. Clark, Search for new physics with atoms and molecules, Rev. Mod. Phys. **90**, 025008 (2018).

[3] V. Giovannetti, S. Lloyd, and L. Maccone, Advances in quantum metrology, Nature Photon **5**, 222 (2011).

[4] A. D. Ludlow, M. M. Boyd, J. Ye, E. Peik, and P. O. Schmidt, Optical atomic clocks, Rev. Mod. Phys. **87**, 637 (2015).

[5] T. Ladd, F. Jelezko, R. Laflamme, Y. Nakamura, C. Monroe, and J. O'Brien, Quantum computers, Nature **464**, 45 (2010).

[6] I. M. Georgescu, S. Ashhab, and F. Nori, Quantum simulation, Rev. Mod. Phys. **86**, 153 (2014).

[7] S. Vinjanampathy and J. Anders, Quantum thermodynamics, Contemporary Physics **57**, 545 (2016).

[8] L. D. Carr, D. DeMille, R. V. Krems, and J. Ye, Cold and ultracold molecules: science, technology and applications, New J. Phys. **11**, 055049 (2009).

[9] J. L. Bohn, A. M. Rey, and J. Ye, Cold molecules: Progress in quantum engineering of chemistry and quantum matter, **357**, 1002 (2017).

[10] D. Demille, Quantum computation with trapped polar molecules, Phys. Rev. Lett. **88**, 067901 (2002).

[11] S. F. Yelin, K. Kirby, and R. Côté, Schemes for robust quantum computation with polar molecules, Phys. Rev. A **74**, 050301 (2006).

[12] K.-K. Ni, T. Rosenband, and D. D. Grimes, Dipolar exchange quantum logic gate with polar molecules, Chem. Sci. **9**, 6830 (2018).

[13] R. Sawant, J. A. Blackmore, P. D. Gregory, J. Mur-Petit, D. Jaksch, J. Aldegunde, J. M. Hutson, M. R. Tarbutt, and S. L. Cornish, Ultracold polar molecules as qudits, New J. Phys. **22**, 013027 (2020).

[14] M. Hughes, M. D. Frye, R. Sawant, G. Bhole, J. A. Jones, S. L. Cornish, M. R. Tarbutt, J. M. Hutson, D. Jaksch, and J. Mur-Petit, Robust entangling gate for polar molecules using magnetic and microwave fields, Phys. Rev. A **101**, 062308 (2020).

[15] R. Barnett, D. Petrov, M. Lukin, and E. Demler, Quantum magnetism with multicomponent dipolar molecules in an optical lattice, Phys. Rev. Lett. **96**, 190401 (2006).

[16] A. Micheli, G. K. Brennen, and P. Zoller, A toolbox for lattice-spin model with polar molecules, Nat. Phys. **2**, 341 (2006).

[17] A. V. Gorshkov, S. R. Manmana, G. Chen, E. Demler, M. D. Lukin, and A. M. Rey, Quantum magnetism with polar alkali-metal dimers, Phys. Rev. A **84**, 033619 (2011).

[18] S. R. Manmana, E. M. Stoudenmire, K. R. A. Hazzard, A. M. Rey, and A. V. Gorshkov, Topological phases in ultracold polar-molecule quantum magnets, Phys. Rev. B **87**, 081106 (2013).

[19] R. V. Krems, Cold controlled chemistry, Physical Chemistry Chemical Physics **10**, 4079 (2008).

[20] N. Balakrishnan, Perpective: Ultracold molecules and the dawn of cold controlled chemistry, Journal of Chemical Physics **145**, 150901 (2016).

[21] M.-G. Hu, Y. Liu, M. A. Nichols, L. Zhu, G. Quéméner, O. Dulieu, and K.-K. Ni, Nuclear spin conservation enables state-to-state control of ultracold molecular reactions, Nature Chemistry 10.1038/s41557-020-00610-0 (2020).

[22] T. Zelevinsky, S. Kotochigova, and J. Ye, Precision test of mass-ratio variations with lattice-confined ultracold molecules, Phys. Rev. Lett. **100**, 043201 (2008).

[23] J. J. Hudson, D. M. Kara, I. J. Smallman, B. E. Sauer, M. R. Tarbutt, and E. A. Hinds, Improved measurement of the shape of the electron, Nature **473**, 493 (2011).

[24] The ACME Collaboration, Improved limit on the electric dipole moment of the electron, Nature **562**, 355 (2018).

[25] J. W. Park, Z. Z. Yan, H. Loh, S. A. Will, and M. W. Zwierlein, Second-scale nuclear spin coherence time of ultracold ^{23}Na^{40}K molecules, Science **357**, 372 (2017).

[26] B. Neyenhuis, B. Yan, S. A. Moses, J. P. Covey, A. Chotia, A. Petrov, S. Kotochigova, J. Ye, and D. S. Jin, Anisotropic polarizability of ultracold polar ^{40}K^{87}Rb molecules, Phys. Rev. Lett. **109**, 230403 (2012).

[27] S. A. Will, J. W. Park, Z. Z. Yan, H. Loh, and M. W. Zwierlein, Coherent microwave control of ultracold ^{23}Na^{40}K molecules, Phys. Rev. Lett. **116**, 225306 (2016).

[28] P. D. Gregory, J. Aldegunde, J. M. Hutson, and S. L. Cornish, Controlling the rotational and hyperfine state of ultracold ^{87}Rb^{133}Cs molecules, Phys. Rev. A **94**, 041403(R) (2016).

[29] J. A. Blackmore, P. D. Gregory, S. L. Bromley, and S. L. Cornish, Coherent manipulation of the internal state of

ultracold ^{87}Rb^{133}Cs molecules with multiple microwave fields, Phys. Chem. Chem. Phys. 10.1039/d0cp04651e (2020).

[30] P. D. Gregory, J. A. Blackmore, J. Aldegunde, J. M. Hutson, and S. L. Cornish, ac stark effect in ultracold polar ^{87}Rb^{133}Cs molecules, Phys. Rev. A **96**, 021402(R) (2017).

[31] J. A. Blackmore, R. Sawant, P. D. Gregory, S. L. Bromley, J. Aldegunde, J. M. Hutson, and S. L. Cornish, Controlling the ac Stark effect of RbCs with dc electric and magnetic fields, Phys. Rev. A **102**, 053316 (2020).

[32] P. K. Molony, P. D. Gregory, Z. Ji, B. Lu, M. P. Köppinger, C. R. Le Sueur, C. L. Blackley, J. M. Hutson, and S. L. Cornish, Creation of ultracold ^{87}Rb^{133}Cs molecules in the rovibrational ground state, Phys. Rev. Lett. **113**, 255301 (2014).

[33] P. K. Molony, P. D. Gregory, A. Kumar, C. R. Le Sueur, J. M. Hutson, and S. L. Cornish, Production of ultracold ^{87}Rb^{133}Cs in the absolute ground state: complete characterisation of the STIRAP transfer, ChemPhysChem. **17**, 3811 (2016).

[34] P. G. H. Sandars, Differential polarizability in the ground state of the hydrogen atom, Proc. Phys. Soc. **92**, 857 (1967).

[35] P. D. Gregory, M. D. Frye, J. A. Blackmore, E. M. Bridge, R. Sawant, J. M. Hutson, and S. L. Cornish, Sticky collisions of ultracold RbCs molecules, Nat. Comms **10**, 3104 (2019).

[36] P. D. Gregory, J. A. Blackmore, S. L. Bromley, and S. L. Cornish, Loss of ultracold ^{87}Rb^{133}Cs molecules via optical excitation of long-lived two-body collision complexes, Phys. Rev. Lett. **124**, 163402 (2020).

[37] X. Ye, M. Guo, M. L. González-Martínez, G. Quéméner, and D. Wang, Collisions of ultracold ^{23}Na^{87}Rb molecules with controlled chemical reactivities, Sci. Adv. **4**, eaaq0083 (2018).

[38] J. F. E. Croft, J. L. Bohn, and G. Quéméner, Unified model of ultracold molecular collisions, Phys. Rev. A **102**, 033306 (2020).

[39] B. Zhu, B. Gadway, M. Foss-Feig, J. Schachenmayer, M. L. Wall, K. R. A. Hazzard, B. Yan, S. A. Moses, J. P. Covey, D. S. Jin, J. Ye, M. Holland, and A. M. Rey, Suppressing the loss of ultracold molecules via the continuous quantum zeno effect, Phys. Rev. Lett. **112**, 070404 (2014).

[40] L. Anderegg, L. W. Cheuk, Y. Bao, S. Burchesky, W. Ketterle, K.-K. Ni, and J. M. Doyle, An optical tweezer array of ultracold molecules, Science **365**, 1156 (2019).

[41] L. W. Cheuk, L. Anderegg, Y. Bao, S. Burchesky, S. S. Yu, W. Ketterle, K.-K. Ni, and J. M. Doyle, Observation of collisions between two ultracold ground-state caf molecules, Phys. Rev. Lett. **125**, 043401 (2020).

[42] J. T. Zhang, Y. Yu, W. B. Cairncross, K. Wang, L. R. B. Picard, J. D. Hood, Y.-W. Lin, J. M. Hutson, and K.-K. Ni, Forming a single molecule by magnetoassociation in an optical tweezer, Phys. Rev. Lett. **124**, 253401 (2020).

[43] R. Bause, M. Li, A. Schindewolf, X.-Y. Chen, M. Duda, S. Kotochigova, I. Bloch, and X.-Y. Luo, Tune-out and magic wavelengths for ground-state ^{23}Na^{40}K molecules, Phys. Rev. Lett. **125**, 023201 (2020).

[44] Y. Liu, M.-G. Hu, M. A. Nichols, G. D. D., T. Karman, H. Guo, and K.-K. Ni, Photo-excitation of long-lived transient intermediates in ultracold reactions, Nat. Phys. **16**, 1132 (2020).

[45] S. Kotochigova and D. DeMille, Electric-field-dependent dynamic polarizability and state-insensitive conditions for optical trapping of diatomic polar molecules, Phys. Rev. A **82**, 063421 (2010).

[46] J. M. Brown and A. Carrington, Rotational Spectroscopy of Diatomic Molecules (Cambridge University Press, 2010).

[47] J. Aldegunde, B. A. Rivington, P. S. uchowski, and J. M. Hutson, Hyperfine energy levels of alkali-metal dimers: Ground-state polar molecules in electric and magnetic fields, Phys. Rev. A **78**, 033434 (2008).

[48] J. Aldegunde and J. M. Hutson, Hyperfine structure of alkali-metal diatomic molecules, Phys. Rev. A **96**, 042506 (2017).

[49] M. P. Köppinger, D. J. McCarron, D. L. Jenkin, P. K. Molony, H. W. Cho, S. L. Cornish, C. R. Le Sueur, C. L. Blackley, and J. M. Hutson, Production of optically trapped ^{87}RbCs Feshbach molecules, Phys. Rev. A **89**, 033604 (2014).

[50] P. D. Gregory, P. K. Molony, M. P. Köppinger, A. Kumar, Z. Ji, B. Lu, A. L. Marchant, and S. L. Cornish, A simple, versatile laser system for the creation of ultracold ground state molecules, New J. Phys. **17**, 055006 (2015).

Figures

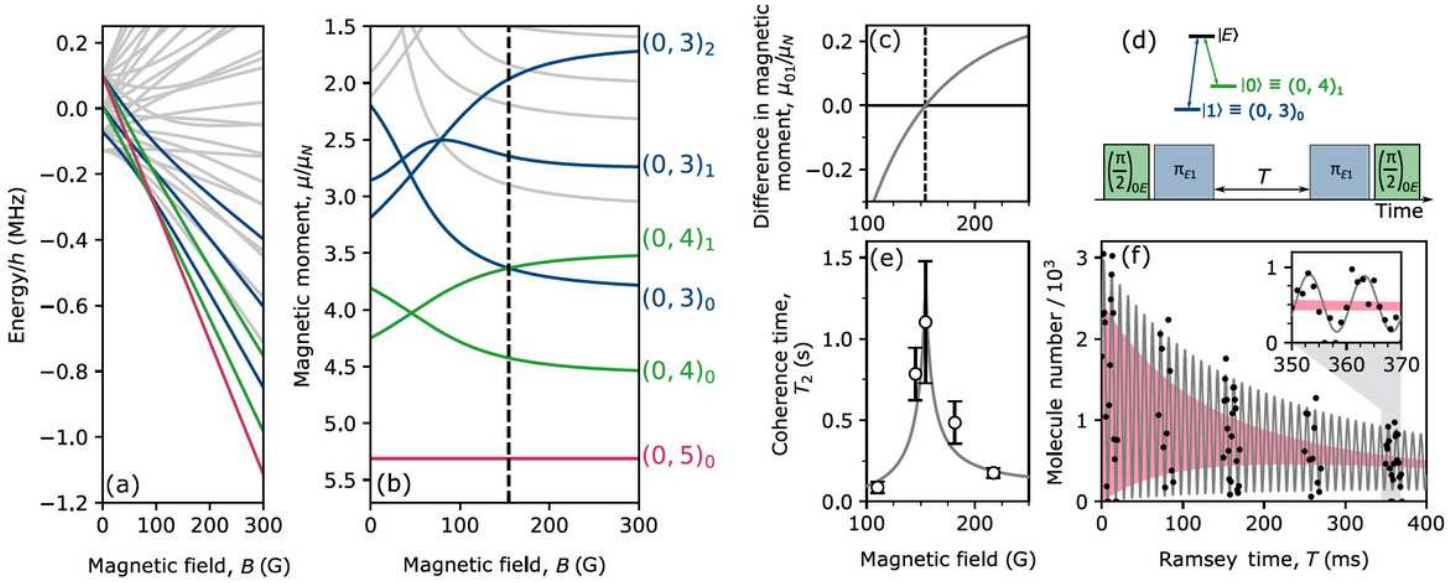

Figure 1

Effect of magnetic fields on the coherence of the storage qubit. (a) Zeeman structure of the nuclear spin states in the rotational ground state of RbCs. (b) Magnetic moments μ/μN of the states as a function of magnetic field B. We construct the qubit from the states |0> ≡ (0, 4)1 and |1> ≡ (0, 3)0, which are chosen as they possess identical magnetic moments when B = 154.524 G (indicated by the vertical dashed line). (c) The differential magnetic moment μ01 = μ|1>−μ|0> as a function of magnetic field. (d) Configuration of states and microwave pulse sequence used to perform Ramsey spectroscopy. The energy separation between the qubit states and the rotationally excited state |E> is 2Bv ≈ 980 MHz. (e) Measured coherence time T2 as a function of magnetic field. The line shows a model for the decoherence as described in the text. Fitting to the results indicates a magnetic field variation of 34(5) mG over the course of the measurement contributes to the observed decoherence, and a peak coherence time T2 = 1.3(4) s when μ01 ≈ 0. (f) Example Ramsey measurement performed at B = 154.50 G, where μ01 ≈ 0. The y-axis indicates the number of molecules remaining in state |0> measured as a function of the Ramsey time T . The red shaded region indicates the maximum and minimum of the Ramsey fringes observed when B = 217.39 G, where μ01 ≈ 0.17 μN and the coherence time is correspondingly much shorter. The trap light has polarisation β = 0 and intensity I = 15.8 kW cm−2 for all measurements shown.

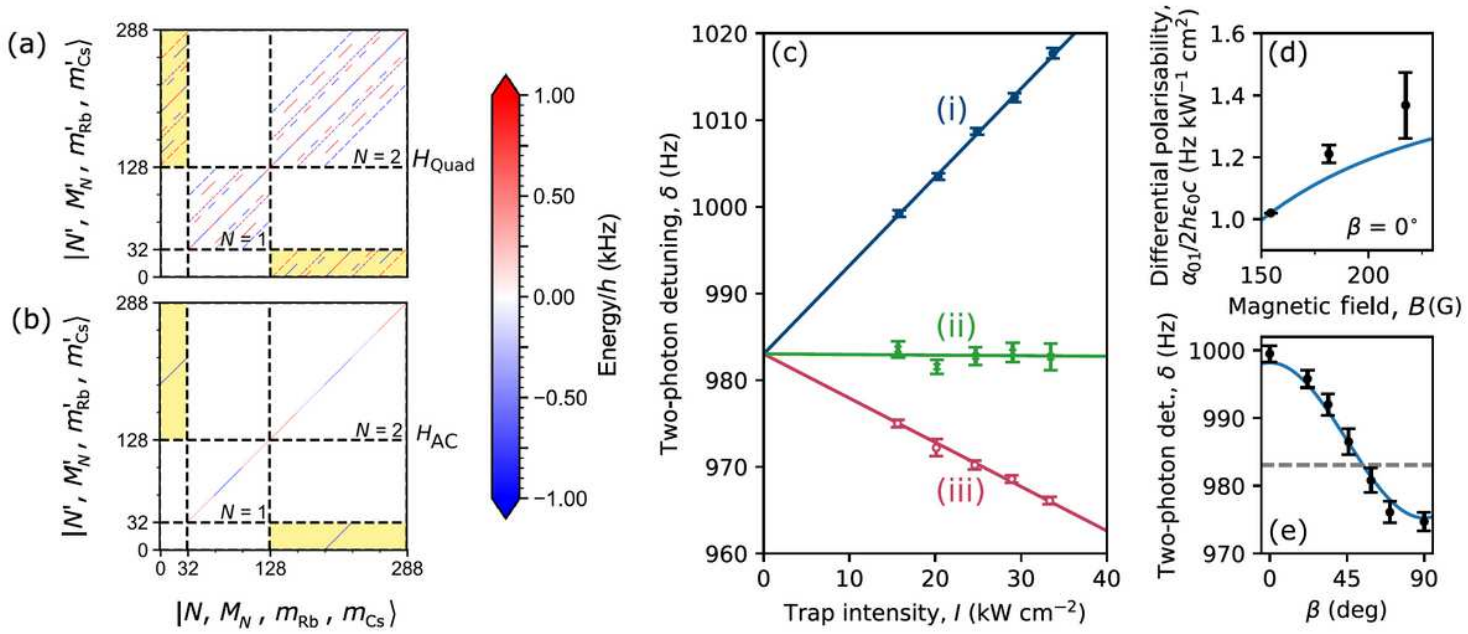

Figure 2

Differential tensor light shifts between nuclear spin states in the rotational ground state. We measure the differential light shifts between |0> ≡ (0, 4)1 and |1> ≡ (0, 3)0 by Ramsey spectroscopy. We show the Hamiltonian matrix elements for (a) the nuclear electric quadrupole interaction Hquad and (b) the AC Stark effect HAC graphically for the uncoupled |N, MN , mRb, mCs> basis. The states are split by dashed lines into groups according to N and by minor ticks into multiples of 32 basis states with the same MN . The block diagonal elements in N are labelled for N > 0. The color coding indicates the value of the matrix element in units of frequency. Note the off-diagonal elements connecting states with ΔN = 2 shaded in yellow, which lead to tensor light shifts proportional to the anisotropic polarisability. The mathematical expressions describing the matrix elements are given in the Supplementary Information. H(2) is calculated for an intensity of 16 kW cm−2 and a polarisation angle of β = 0°. (c) Two-photon detuning δ as a function of the trap intensity I. The linear polarisation of each beam is set to an angle β of (i) 0° (ii) 55° (iii) 90° with respect to a 154.50 G magnetic field. The coloured lines indicate a fit to the results, following the model given in Eq. 3. We find α(2)/(4πe0) = 545(4) a , and δ0 = 983.0(2) Hz. (d) Differential polarisability between the states as a function of magnetic field, measured for β = 0°. The line is the expectation from the molecular Hamiltonian (see Methods). (e) δ measured in a single beam of the dipole trap with fixed intensity I = 15.3 kW cm−2, as a function of β. The dashed horizontal line indicates δ0. The solid line is calculated using Eq.3 with the parameters found in (c).

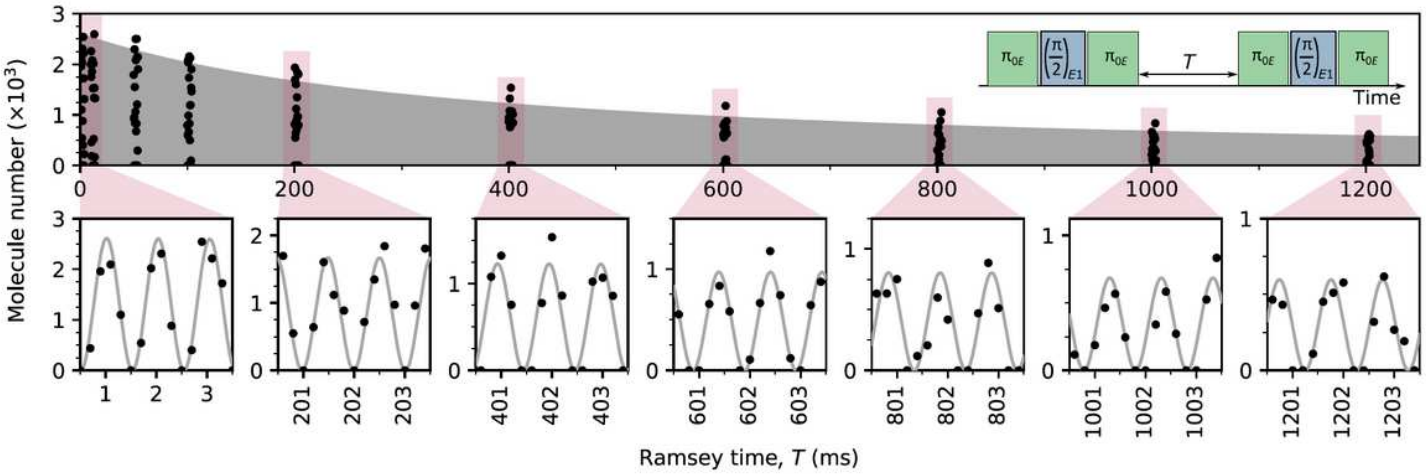

Figure 3

Robust coherence of the storage qubit. Ramsey experiment with the qubit states |0> ≡ (0, 4)1 and |1> ≡ (0, 3)0, using the optimal configuration B ≈ 154.50 G, β ≈ 55°. The y-axis indicates the number of molecules remaining in |0>, following the Ramsey sequence shown inset, as a function of the hold time T . The shaded region in the upper plot indicates the maximum and minimum of the Ramsey fringes as a function of time; the spacing of the fringes is too small to plot at this scale. The lower plots show the Ramsey fringes observed at 400 ms intervals.

Supplementary Files

This is a list of supplementary files associated with this preprint. Click to download.

- Supplementary.pdf